Towards a transcriptome-based theranostic platform for unfavorable breast cancer phenotypes

Andrey S. Dobroff[a,b,1], Sara D'Angelo[a,b,1], Bedrich L. Eckhardt[c,1], Fortunato Ferrara[a,b], Daniela I. Staquicini[a,b], Marina Cardó-Vila[a,b], Fernanda I. Staquicini[a,b], Diana N. Nunes[d], Kisu Kim[e], Wouter H. P. Driessen[f], Amin Hajitou[g], Lesley C. Lomo[a,h], Marc Barry[a,h], Savitri Krishnamurthy[i], Aysegul Sahin[i], Wendy A. Woodward[j], Eric R. Prossnitz[a,b], Robin L. Anderson[k], Emmanuel Dias-Neto[d,l], Ursa A. Brown-Glaberman[a,m], Melanie E. Royce[a,m], Naoto T. Ueno[c], Massimo Cristofanilli[n], Gabriel N. Hortobagyi[c], Serena Marchiò[a,b,o,p], Juri G. Gelovani[q], Richard L. Sidman[r,2], Wadih Arap[a,m,2,3], and Renata Pasqualini[a,b,2,3]

aUniversity of New Mexico Comprehensive Cancer Center, Albuquerque, NM 87131; bDivision of Molecular Medicine, Department of Internal Medicine, University of New Mexico School of Medicine, Albuquerque, NM 87131; cDepartment of Breast Medical Oncology, The University of Texas M. D. Anderson Cancer Center, Houston, TX 77030; dInternational Research Center, A. C. Camargo Cancer Center, Sao Paulo 01508-010, Brazil; eMOGAM Biotechnology Institute, Yongin, Gyeonggi-do 16924, Korea; fDavid H. Koch Center, The University of Texas M. D. Anderson Cancer Center, Houston, TX 77030; gHammersmith Hospital Campus, Imperial College London, London W12 0NN, United Kingdom; hDepartment of Pathology, University of New Mexico School of Medicine, Albuquerque, NM 87131; iDepartment of Pathology, The University of Texas M. D. Anderson Cancer Center, Houston, TX 77030; jDepartment of Radiation Oncology, The University of Texas M. D. Anderson Cancer Center, Houston, TX 77030; kDepartment of Oncology, Sir Peter MacCallum Cancer Centre, The University of Melbourne, Parkville, VIC 3010, Australia; lInstitute of Psychiatry, University of São Paulo Medical School, Sao Paulo 01060-970, Brazil; mDivision of Hematology/Oncology, Department of Internal Medicine, University of New Mexico School of Medicine, Albuquerque, NM 87131; nRobert H. Lurie Comprehensive Cancer Center, Feinberg School of Medicine, Northwestern University, Chicago, IL 60611; oCandiolo Cancer Institute-Fondazione del Piemonte per l'Oncologia, Istituto di Ricovero e Cura a Carattere Scientifico, Candiolo, Turin 10060, Italy; pDepartment of Oncology, University of Turin, Candiolo, Turin 10060, Italy; qDepartment of Biomedical Engineering, Wayne State University, Detroit, MI 48201; and rDepartment of Neurology, Beth Israel Deaconess Medical Center, Harvard Medical School, Boston, MA 02215

Inflammatory breast carcinoma (IBC) is one of the most lethal forms of human breast cancer, and effective treatment for IBC is an unmet clinical need in contemporary oncology. Tumor-targeted theranostic approaches are emerging in precision medicine, but only a few specific biomarkers are available. Here we report up-regulation of the 78-kDa glucose-regulated protein (GRP78) in two independent discovery and validation sets of specimens derived from IBC patients, suggesting translational promise for clinical applications. We show that a GRP78-binding motif displayed on either bacteriophage or adeno-associated virus/phage (AAVP) particles or loop-grafted onto a human antibody fragment specifically targets orthotopic IBC and other aggressive breast cancer models in vivo. To evaluate the theranostic value, we used GRP78-targeting AAVP particles to deliver the human *Herpes simplex* virus thymidine kinase type-1 (*HSVtk*) transgene, obtaining simultaneous in vivo diagnosis through PET imaging and tumor treatment by selective activation of the prodrug ganciclovir at tumor sites. Translation of this AAVP system is expected simultaneously to image, monitor, and treat the IBC phenotype and possibly other aggressive (e.g., invasive and/or metastatic) subtypes of breast cancer, based on the inducible cell-surface expression of the stress-response chaperone GRP78, and possibly other cell-surface receptors in human tumors.

inflammatory breast cancer | ligand-directed theranostics | molecular imaging | gene therapy | AAVP

Breast cancer remains a major cause of cancer death in women (1), and one of its most lethal presentations is inflammatory breast carcinoma (IBC), a clinicopathological diagnosis characterized by diffuse erythema/edema involving the skin of the breast (a sign classically known as "*peau d'orange*") caused by tumor emboli within the dermal lymphatics. Although IBC comprises <5% of breast cancer cases, the tumor accounts for more than 10% of breast cancer mortality in the United States (2, 3). IBC is considered aggressive because it evolves rapidly—over days to weeks rather than months—with most patients presenting with lymph node involvement and more than 30% of patients having distant metastases at diagnosis (4, 5). Although IBC, like non-IBC breast cancers, is a heterogeneous disease and can occur as any of the five molecular subtypes, the IBC is most commonly ErbB2 overexpressing or triple negative (6), thus rendering a large armamentarium of targeted drugs ineffective. Finally, IBC generally presents with high-grade histology, elevated cell proliferation rate, and

angiolymphatic invasion (5, 7). Indeed, the hallmark lymphatic invasion dictates the requirement for initial systemic treatment of IBC, because micrometastatic disease likely has occurred even in the

Significance

Inflammatory breast cancer (IBC) is defined clinically and pathologically. Dermal lymphatic invasion is typical but is neither necessary nor sufficient for diagnosis; sentinel lymph node biopsy is contraindicated, challenging multidisciplinary management with upfront chemotherapy, surgery, and postoperative radiotherapy. Here we applied a ligand-directed "theranostic" (a combination of therapeutic and diagnostic) enabling platform to target IBC based on adeno-associated virus/phage (AAVP)-*Herpes simplex* virus thymidine kinase type-1 (*HSVtk*) particles displaying ligands to cell surface-associated 78-kD glucose-regulated protein (GRP78). In a suite of preclinical models and human tumor samples, we show simultaneous non-invasive molecular serial PET/CT imaging and targeted suicide transgene therapy. This study shows that a tumor-specific promoter, human *GRP78* (*hGRP78*), can drive the expression of an imaging/suicide transgene in IBC and aggressive breast cancer in vivo.

absence of overt metastasis, as evidenced by the high incidence of tumor recurrence. Aggressive local management with surgery and nodal radiotherapy typically follows systemic combination chemotherapy (4–7). Collectively, the pathological and molecular underpinnings of the disease contribute to the poor prognosis of IBC patients relative to other, more common subtypes of human breast cancer (8). Therefore IBC is unequivocally considered a formidable clinical challenge in contemporary cancer medicine (2–8). Within this clinical context, the emerging field of "theranostic" (a combination of the terms "therapeutic" and "diagnostic") approaches offers an attractive avenue for the concurrent detection and treatment of cancer. We previously have developed targeted hybrids of adeno-associated virus and phage particles (AAVP), functional vectors that enable synchronous ligand-directed and transcriptional delivery of transgenes (9). In the decade since their introduction, we have validated the delivery of therapeutic genes via peptide-directed AAVP vectors to xenograft and transgenic models of tumors such as soft-tissue sarcomas (10), glioblastomas (11), pancreatic neuroendocrine tumors (12), and even to dogs with various native tumors (13).

In the present study, the AAV component of the particle provides a theranostic agent, the human *Herpes simplex virus thymidine kinase type-1* (*HSVtk*) gene, for molecular–genetic imaging and/or suicide gene therapy, and the phage component of the particle incorporates the targeting moiety, a short ligand peptide motif expressed as an in-frame fusion within the minor capsid protein (pIII) (9). As a proof of concept for ligand-directed theranostics in IBC, we have chosen 78-kD glucose-regulated protein (GRP78) as a promising tumor target in human breast cancer (14). Under physiological conditions, GRP78 is expressed in the endoplasmic reticulum with pleomorphic functions in protein folding and assembly (15); however, as a stress-response chaperone in cancer (16), GRP78 relocalizes to the cell surface (17). Our group originally demonstrated that cell-surface GRP78 enables tumor targeting by circulating ligands in vivo (18, 19), an observation confirmed by independent investigators (20, 21). Both hormone receptor-positive and -negative breast cancers appear to overexpress GRP78 (22, 23), and high levels of GRP78 in patients correlate to poor responses to chemotherapy and lower survival rates (24). However, despite its promise as a functional molecular target and as a potential prognostic marker in human breast cancer, the role of GRP78 in patients with IBC remains unclear, hence the impetus for this work.

Here we investigated the presence of cell-surface GRP78 in the context of human IBC, explored the theranostic value of ligand peptide-directed AAVPs or motif loop-grafted monoclonal antibody fragments, and compared the potency of the cognate human GRP78 native stress-inducible promoter (*hGRP78*) to that of constitutive *CMV* promoter-based transcription. In several relevant preclinical models of IBC, ligand-directed and transcriptional targeting of GRP78 provided efficient tumor visualization by PET imaging as well as the selective cellular destruction of orthotopic IBC tumors, with minimal off-target activity detected. Taken together, these results represent a meaningful step toward the translation into clinical practice of an AAVP-based ligand-directed and transcriptional theranostics against IBC and potentially against other aggressive breast cancers.

Results

GRP78 Is Strongly Expressed in Human IBC. To evaluate the protein levels of GRP78 in human IBC systematically, we examined GRP78 expression by immunohistochemistry (IHC) on a discovery set of index IBC patients (*n* = 5) who underwent surgery at the University of New Mexico Comprehensive Cancer Center (UNMCCC). Having observed moderate-to-strong positivity for GRP78 in this small pilot study (Fig. 1 *A–F*), we next investigated protein levels in a relatively larger validation set (*n* = 20) from representative IBC patients having surgery at The University of Texas M. D. Anderson Cancer Center (MDACC), with similar results (Fig. 1 *G–L*). Staining of the initial discovery set revealed moderate-to-strong positivity in two index cases (Fig. 1 *A* and *C*) and moderate positivity in three index cases (Fig. 1*E*), suggesting

the presence of this protein on the cell surface as demonstrated by our previous study (19). The validation set from the MDACC confirmed similar patterns, with moderate-to-strong GRP78 levels (Fig. 1 *H* and *I*); intense GRP78 expression was detected in tumor cells infiltrating white adipose tissue (Fig. 1*J*) or tumor stroma (Fig. 1*K*) as well as in lymph node metastases (Fig. 1*L*). Together, results from these independent datasets provide evidence that GRP78 is a candidate molecular target in IBC.

A GRP78-Targeting Peptide Motif Is a Ligand for IBC- and Aggressive Breast Cancer-Derived Cells. To gain quantitative functional targeting insight (Fig. 2), we initially characterized the selective binding of the GRP78-binding peptide motif WIFPWIQL (19) to a representative panel (*n* = 9) of immortalized breast epithelial cells and tumorigenic breast cancer cells in vitro. We assessed the binding of phage particles displaying WIFPWIQL and control (insertless) phage particles to tumorigenic cell lines recapitulating different breast cancer subtypes, including primary invasive ductal (human, BT474), invasive/metastatic [human, SK-BR-3, MCF7, MDA-MB-231; murine, 4T1.2, EF43.*fgf4* (25)], and IBC [human, MDA-IBC-3, SUM190 (26, 27)] breast cancer cells and also to a nontumorigenic mammary cell line (human, MCF10A). Phage binding was evaluated by the BRASIL (biopanning and rapid analysis of selective interactive ligands) methodology (28) and revealed a particularly marked interaction of GRP78-targeting phage particles with the cell surface of human IBC and murine highly aggressive breast cancer cell lines (Fig. 2*A*). This interaction was inhibited significantly (*P* < 0.05 by two-tailed Student's *t* test) after incubation with a neutralizing anti-GRP78 antibody (Fig. 2*B*), indicating a specific interaction between the WIFPWIQL peptide and cell-surface GRP78. Consistent with this finding, flow cytometry analysis revealed abundant cell surface-associated GRP78 expression in the human and murine lines, as shown in Fig. 2*C* for SUM190 cells, further corroborating the value of GRP78 as a cell-surface receptor target in human IBC.

Ligand-Directed Imaging of IBC-Bearing Mice. To investigate whether cell-surface–associated GRP78 targeting could be exploited in ligand-directed strategies for in vivo imaging, we next completed experiments with near-infrared (NIR)-based tracing of fluorescently labeled phage. Either GRP78-targeting or control phage particles were conjugated side-by-side to an infrared dye (RDye 800CW) and subsequently were administered i.v. to orthotopic SUM190 IBC-bearing mice (*n* = 5 mice per group). Phage particles were imaged by whole-body NIR fluorescence (NIRF) and revealed specific localization of GRP78-targeting particles to established IBC xenografts (Fig. 3*A*). As expected, nonspecific phage accumulation was equally detected in the hepato-splenic organs because of the documented retention of phage within the reticuloendothelial system (29–31) (see *SI Discussion* for further discussion of the potential for AAVP in the clinical setting), regardless of the peptide displayed, and served as an additional internal control. Relative quantification of tumor-associated signals revealed a sixfold higher intensity of GRP78-targeting phage homing than control phage homing (Fig. 3*B*). These data confirm that circulating phage particles displaying a GRP78-targeting peptide localized specifically to tumor lesions in a preclinical model of IBC.

To ensure that the ligand motif WIFPWIQL (19) would target cell-surface GRP78 in vivo outside of the context of phage particles (in which up to five recombinant peptide motifs are displayed in pIII), we next loop-grafted the GRP78-targeting peptide into a human fragment antigen-binding (Fab) backbone to obtain a convenient standard entity that retains the GRP78-binding attributes, exhibits inherent biological stability, and has a single antigen-binding site, thus ruling out the possibility that peptide avidity (rather than affinity) might account for GRP78-targeting phage homing in vivo. The loop-grafted GRP78-targeting Fab was initially evaluated by ELISA and showed concentration-dependent binding to immobilized human recombinant GRP78 relative to a control Fab (Fig. 4*A*). We next evaluated the in vivo efficacy of this GRP78-targeting Fab in mouse isogenic EF43.*fgf4* mammary tumors (25), enabling us also to evaluate the efficacy
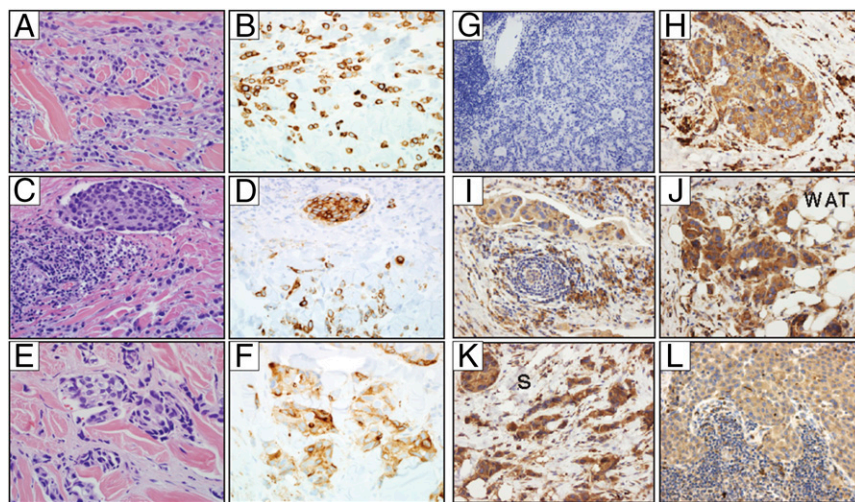
Fig. 1. GRP78 protein levels in specimens derived from human IBC patients. Archival formalin-fixed paraffin-embedded (FFPE) tissue slides from IBC patients were stained with anti-GRP78 antibody, and signals were revealed with a 3,3'-diaminobenzidine-tetrahydrochloride (DAB) substrate. (*A–F*) Discovery set. Invasive mammary carcinoma in representative biopsies from patients with clinically diagnosed IBC. (*A*, *C*, and *E*) H&E staining. (*B*, *D*, and *F*) Immunohistochemical staining for GRP78. (Magnification: 40×.) (*G–L*) Validation set. (*G*) Negative control (isotype antibody). (*H* and *I*) Representative primary IBC samples. (*J*) Representative IBC within white adipose tissue (WAT). (*K*) Representative IBC within stroma (S). (*L*) Representative metastasis-positive lymph node. (Magnification: *G*, 10×; *H–L*, 20×.)

of the WIFPWIQL motif across different in vivo models. This model was selected because of its pathological similarity to the clinical disease, including a high level of inflammation, extensive angiogenic potential, rapid proliferation, and local invasion in an animal with an intact immune system. The IRDye 800CW-labeled GRP78-targeting Fab was administered i.v. (20 µg per mouse) to mice bearing orthotopic implants of EF43.*fgf4* tumor cells, followed by evaluation of NIR signals at different time points. Within the context of this model, the tumor was specifically imaged by whole-body NIRF with the GRP78-targeting Fab but not with the control Fab (Fig. 4*B*). Quantification of signal at the tumor site showed a significant threefold increase in fluorescence (Fig. 4*C*) that persisted up to 72 h (*P* < 0.05 relative to the control Fab, by two-tailed Student's *t* test). Collectively, these results confirm the reliability of a single binding unit of the GRP78-targeting peptide WIFPWIQL in a preclinical IBC model, regardless of the scaffold displaying the peptide motif.

Cell-Surface GRP78-Targeting Theranostics Based on Ligand-Directed AAVP Particles. Having characterized the binding attributes of the WIFPWIQL motif, we next engineered GRP78-targeting AAVP particles (9, 32) to enable theranostic function in preclinical models of human IBC in immunodeficient mice and in aggressive mouse mammary cancers in immunocompetent mice. Briefly, we inserted into the M13-based phage genetic backbone an AAV genomic cassette containing the *HSVtk* transgene under the control of either the standard constitutive and highly efficient *CMV* promoter or the stress-inducible human GRP78 (*hGRP78*)-selective promoter (33, 34) to compare the two promoters directly in vivo. In this system, the *HSVtk* transgene may function as a serial noninvasive molecular–genetic imaging sensor and reporter in the presence of specific radiolabeled substrates (35). We

administered either GRP78-targeting or control AAVP particles to mice bearing SUM190 orthotopic tumors. Mice received control or GRP78-targeting AAVP on days 0 and 5, and *HSVtk* expression was assessed on days 6 and 16 by whole-body PET imaging immediately after i.v. administration of the [^{124}I]-2-fluoro-5-iodo-1-β-D-arabino-furanosyl-uracil ([^{124}I]-FIAU) substrate (Fig. 5*A*) (34). Compared with the *CMV* promoter, the *hGRP78* promoter conferred much higher tumor-detection sensitivity to the GRP78-targeting AAVP, in terms of signal-to-noise ratio (Fig. 5*B*, whole-body PET, and Fig. 5*C*, tumor-associated signal quantification). The low background signal in the control is caused by the affinity of [^{124}I]-FIAU for endogenous thymidine kinases, especially in highly proliferative tumor cells in which TK1 is particularly active. Longitudinal radial profiles of explanted tumors (Fig. 5*D*) from IBC-bearing mice receiving GRP78-targeting (either *CMV* or *hGRP78* promoter) or control AAVP revealed significant ligand-directed tumor accumulation of both vectors (*P* < 0.05 by two-way ANOVA followed by Bonferroni's test) at day 16 after AAVP administration (Fig. 5*E*), when the experiment was terminated. No off-target *HSVtk* activity was detected in organs that did not have lesions, including muscle, kidney, heart and liver (Fig. 5*F*), thus indicating targeting specificity. Collectively, these spatiotemporal quantitative data in preclinical settings establish the value of targeting GRP78 for noninvasive serial molecular–genetic imaging of IBC.

Having demonstrated the diagnostic attributes of targeting cell-surface GRP78 with AAVP constructs in IBC, we next evaluated the therapeutic potential of this ligand-directed theranostic platform technology. AAVP-transduced *HSVtk* also may act as a cell suicide-inducing gene in the presence of ganciclovir (GCV), which is converted by the thymidine kinase enzyme to a cytotoxic compound (36). To investigate the efficacy of the GRP78-targeting AAVP in breast cancer treatment, we used the syngeneic EF43.*fgf4*
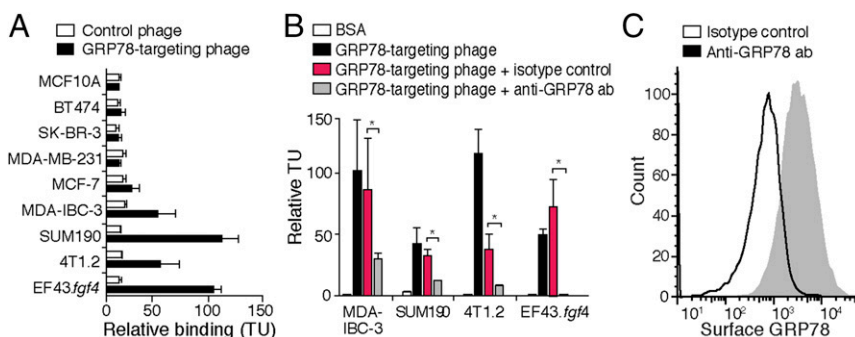
Fig. 2. Specificity of GRP78-targeting phage particles. (*A*) Phage binding to human breast cancer and murine mammary tumor cell lines. (*B*) Binding specificity of GRP78-targeting phage particles was evaluated in competition assays in the presence of an anti-GRP78 antibody in representative human IBC (MDA-IBC-3, SUM190) and murine mammary tumor (4T1.2, EF43.*fgf4*) cell lines. Rabbit immunoglobulins served as an isotype antibody negative control, and BSA served as a negative protein control. Phage binding is displayed as mean ± SEM; *P < 0.05 relative to control antibody incubation, by two-tailed Student's *t* test. (*C*) Representative flow cytometry analysis of cell-surface GRP78 expression in human IBC cells (SUM190).
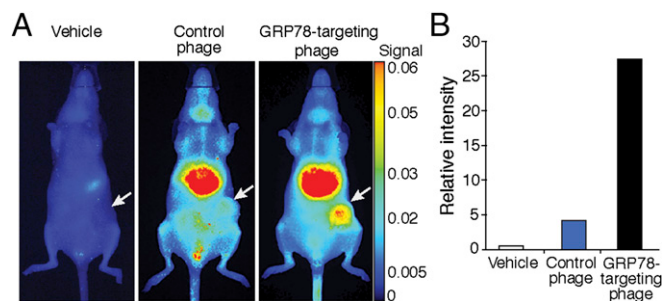
Fig. 3. NIR-labeled GRP78-targeting phage particles for preclinical imaging of human IBC xenografts. (*A*) Human SUM190 orthotopic IBC-bearing nude mice (*n* = 5 per group) received vehicle only, fluorescent control phage, or GRP78-targeting phage particles. Fluorescence images were obtained 24 h after injection. Arrows indicate tumor localization (ventral view). (*B*) Relative quantification of fluorescence signals at the SUM190 cell-derived tumor xenograft site.

mammary tumor model (25, 37). Five days after tumor cell implantation, mice received an i.v. dose of GRP78-targeting AAVP particles (with either the *CMV* or the *hGRP78* promoter), control AAVP particles, or vehicle-only (PBS) as negative controls. After 3 d, mice underwent daily GCV treatment for 7 d, and tumor growth rates were monitored throughout the experiment, for a total of 15 d. Given the high morbidity and mortality of mice bearing EF43.*fgf4* tumors, we could not extend these therapeutic experiments for more than 10 d after AAVP administration because of large tumor burden or lethality in controls. Mice with size-matched tumors that received GRP78-targeting AAVP particles (with either the *CMV* or the *hGRP78* promoter) showed significant tumor reduction compared with the control groups (Fig. 6*A*). The evaluation of explanted tumors at the end point confirmed a significant decrease in tumor growth for animals treated with either GRP78-targeting AAVP, with a mean reduction in tumor volume of 20% for AAVP constructs carrying the *CMV* promoter and 46% for AAVP constructs carrying the *hGRP78* promoter (*P* < 0.01 and 0.001, respectively, relative to the control AAVP, by two-way ANOVA followed by Bonferroni's test) (Fig. 6*B*). These data show that targeting cell-surface GRP78 with AAVP particles is an efficient strategy for GCV-based suicide therapy against experimental breast cancer. Overall, the results reported in Figs. 5 and 6 demonstrate the value of ligand-directed theranostic AAVP approaches.

Discussion

Here we report a proof-of-concept experiment for a ligand-directed theranostic-enabling platform that is readily translatable into clinical applications for diagnosis and therapy of IBC.

The presence of systemically accessible tumor- and/or vascular endothelial cell-specific surface receptors is expected to favor the targeted delivery of active imaging agents and/or therapeutic drugs (38), with consequent improvement in therapeutic indices and with reduced side effects. The possibility of enhancing drug efficacy by concentrating an active agent at the tumor site therefore is a promising alternative for aggressive breast cancer therapy; however, only a small number of tumor-specific receptors have been identified so far. Chaperone heat-shock and glucose-regulated proteins have only recently—and quite unexpectedly—been described as abundant (protein "moonlighting") on tumor and neovascular cell surfaces (16–18). Among these proteins, GRP78 is part of an evolutionarily conserved endoplasmic reticulum-linked stress-response mechanism that provides survival signals during environmental and physiologic stress (39). GRP78 is classically involved with the processing of unfolded proteins (15); however, recent mechanistic insights also place this protein at the cell surface with the potential to influence signal transduction (40, 41). GRP78 has been targeted previously for anticancer treatment (42, 43). Indeed, our group has reported GRP78 overexpression in a limited set of matched primary/metastatic tumors from patients with prostate and breast

cancer, supporting the likelihood of systemic targeting of surface GRP78 in primary and metastatic disease settings (44, 45).

Based on these considerations, we developed a ligand-directed AAVP (9) for noninvasive serial imaging and suicide gene therapy of IBC and for other aggressive breast cancer subtypes in which GRP78 is highly expressed and in which the protein is accessible because of its translocation to the tumor cell surface. In the treatment of highly invasive tumors, the availability of new theranostic tools using molecular–genetic imaging is critical for early diagnosis and for a rapid change in therapy upon the development of resistance. In particular, given that IBC is often misdiagnosed because of its atypical disease presentation and/or is understaged because of the early onset of micrometastasis before distant disease can be documented (4, 5), an effective molecular methodology for early tumor detection, staging, and serial monitoring of response and local or distant disease recurrence clearly remains an unmet medical need. Attesting to its inherent versatility, ligand-directed AAVP-based delivery of transgenes in preclinical settings has been demonstrated successfully in xenograft and transgenic models of soft-tissue sarcomas (10), glioblastomas (11), and neuroendocrine pancreatic tumors (12), in addition to the original new technology report in breast and prostate cancer in tumor-bearing mice a decade ago (9, 19). Notably, one also could speculate that the described ligand-directed theranostic approach introduced here could also be used to determine the precise location of a lesion intraoperatively and/or to integrate the administration of tumor-directed treatments based on the recent report of an enabling AAVP-based nanotechnology platform (46). (See *SI Discussion* for a further discussion of the potential for AAVP in the clinical setting.)

In aggressive human cancer subtypes, such as IBC, for which precision medicine treatments are urgently needed but lacking, our strategy is attractive for future clinical applications, given the possibility of coupling noninvasive imaging for serial biopsy-free disease monitoring to treatment in a single i.v. administration. We propose the use of the *hGRP78* promoter as an effective and specific transational transcription-directed strategy as demonstrated
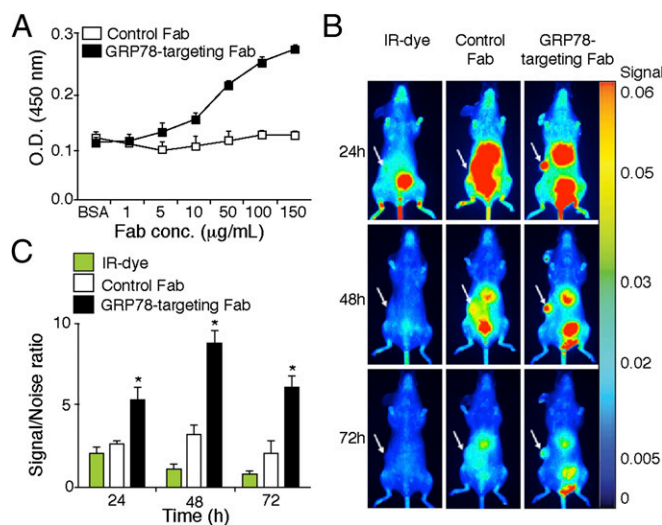
Fig. 4. NIR-labeled GRP78-targeting Fab for preclinical imaging of breast cancer xenografts. (*A*) Binding specificity of the Fab loop-engrafted GRP78-targeting peptide was assessed in vitro by ELISA on immobilized human recombinant GRP78. BSA served as a negative control protein. (*B*) EF43.*fgf4* orthotopic breast cancer-bearing mice (*n* = 5 per group) received i.v. IRDye 800CW alone (IR-dye), IRDye 800CW-labeled control Fab, or IRDye 800CW-labeled loop-grafted GRP78-targeting Fab. Images were obtained serially at 24, 48, and 72 h after administration. Arrows indicate tumor xenograft localization (ventral view). (*C*) Relative signal quantification is represented as the signal-to-noise ratio of the indicated treatments to autofluorescence at the tumor site after 24, 48, and 72 h. Results are represented as mean ± SEM; **P* < 0.05 relative to control Fab, by two-tailed Student's *t* test.
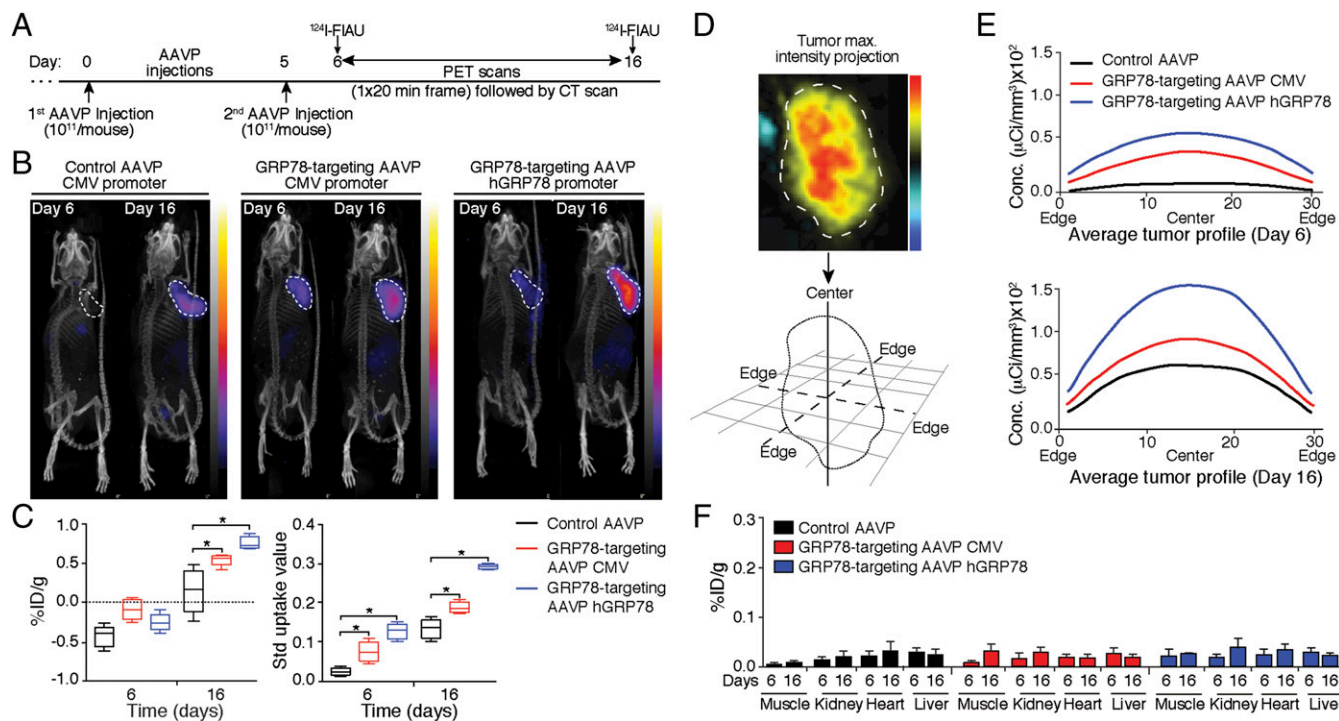
Fig. 5. Molecular–genetic imaging based on GRP78-targeting AAVP in a preclinical model of human IBC. (*A*) Scheme of time points of AAVP administration, [^{124}I]-FIAU dosing, and PET/CT imaging acquisition. A representative IBC model of human SUM190 tumor xenografts in nude mice was used. (*B*) Maximum intensity full-body projections of tumor-bearing mice receiving control AAVP with the *CMV* promoter, GRP78-targeting AAVP with the *CMV* promoter, or GRP78-targeting AAVP with the *hGRP78* promoter. Representative PET/CT images are shown. Images were acquired at day 6 and day 16 after the first AAVP administration. All PET images shown are set out to 3% injected dose per gram of tissue (ID/g). Dashed lines indicate the tumor location. (*C*) Group average tumor xenograft concentrations (*Left*) and standard tumor xenograft uptake (*Right*) (normalized to baseline, *P < 0.05 by two-way ANOVA followed by Bonferroni's test). In the box-and-whiskers plots the horizontal line represents the median, the box represents quartiles, and whiskers represent 5–95% confidence limits. (*D*) Representative longitudinal radial profile of AAVP particle distribution within tumor xenografts. (*E*) Average [^{124}I]-FIAU concentration (tumor profile plot) at day 6 (*Upper*) and day 16 (*Lower*) for tumors treated with control AAVP with the *CMV* promoter, GRP78-targeting AAVP with the *CMV* promoter, or GRP78-targeting AAVP with the *hGRP78* promoter. (*F*) AAVP biodistribution: average [^{124}I]-FIAU concentration in tumor-negative control tissues at day 6 and day 16.

by the clear molecular–genetic imaging results and a trend in the therapeutic results presented in this work. The benefits of the *hGRP78* promoter reside not only in its specific activation in GRP78-expressing tumor cells but also in the persistence of *HSVtk* gene expression over the *CMV* promoter, which may be subjected to silencing by eukaryotic cells (33, 34). Moreover, because GRP78 is a stress-induced protein, one could predict that the harsh tumor microenvironment would increase GRP78 transcription in a positive feedback loop that would potentiate protein production, cell-surface relocalization, and, ultimately, the availability and accessibility of this molecular target. Notably, the advantage of the *hGRP78* promoter is expected to be evident when translated to patients, in whom the effects can be evaluated over long periods of time (several weeks to months) rather than in the mere 10-d framework possible in our preclinical therapeutic experiments.

In conclusion, in the present work we designed and introduced a GRP78-targeting theranostic system and have validated it in multiple preclinical settings. If translational applications are successfully developed, the platform can be exploited for highly specific molecular–genetic imaging and treatment of IBC and potentially other aggressive human breast cancer subtypes. Gene therapy has been recognized as a great promise for the treatment of cancer, but the lack of a robust system to deliver reporter and/or therapeutic transgene(s) effectively and specifically is a serious limiting factor. The AAVP-based strategy reported here has its maximum diagnostic and therapeutic efficacy targeted at the tumor site, making it a promising candidate for the development of first in-human clinical trials for tumors such as IBC and aggressive variant prostate cancer (46), which are in the advanced planning stage. Finally, in the future other tumor-specific ligand-

receptor systems and/or inducible promoters may be integrated easily into the AAVP-based platform.
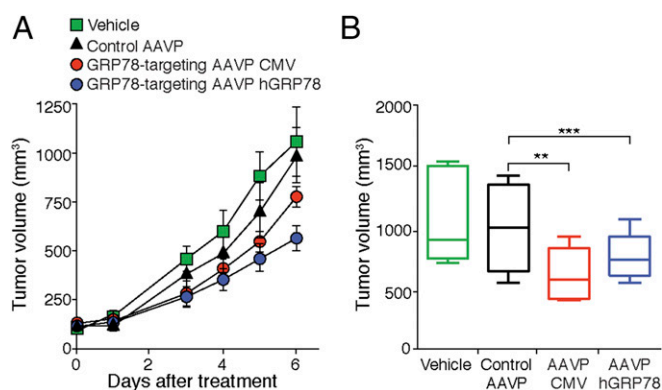
Fig. 6. Therapeutic approach with cell suicide-inducing transgene delivery by GRP78-targeting AAVP in a preclinical model of highly aggressive breast cancer. (*A*) EF43.*fgf4* orthotopic breast cancer-bearing mice (*n* = 6 per group) received vehicle only, control AAVP, or GRP78-targeting AAVP with either the *CMV* or the *hGRP78* promoter to drive the *HSVtk* gene expression. GCV was administered daily starting 3 d after AAVP administration. (*B*) Explanted tumor volumes at the end of the experiments. Shown are the mean tumor volumes at day 6 of GCV treatment in mice that received vehicle only, control AAVP, or GRP78-targeting AAVP with either the *CMV* or the *hGRP78* promoter: 508 ± 65, 753 ± 52, and 940 ± 95 mm³, respectively. **P < 0.01, ***P < 0.001 relative to the control AAVP, by two-way ANOVA followed by Bonferroni's test.

MEDICAL SCIENCES

Materials and Methods

This study adheres strictly to current medical ethics recommendations and guidelines on human research and has been reviewed and approved by the Clinical Ethics Service, Institutional Biohazard Committee, Clinical Research Committee, and Institutional Review Board at the corresponding institutions. The animal experiments reported in this paper were conducted in full compliance with MDACC Institutional Animal Care and Utilization Committee (IACUC) policies and procedures, which follow a strict current guide care and use of laboratory animals (47). Before the initiation of experiments, all protocols and procedures involving animals were reviewed and approved by the IACUC of the site performing the experiment.

Reagents and all experimental procedures, such as the design of targeted AAVP and all in vivo and in vitro applications, are fully described in *SI Materials and Methods*.

1. DeSantis CE, et al. (2016) Breast cancer statistics, 2015: Convergence of incidence rates between black and white women. *CA Cancer J Clin* 66(1):31–42.
2. Woodward WA (2015) Inflammatory breast cancer: Unique biological and therapeutic considerations. *Lancet Oncol* 16(15):e568–e576.
3. Hance KW, Anderson WF, Devesa SS, Young HA, Levine PH (2005) Trends in inflammatory breast carcinoma incidence and survival: The surveillance, epidemiology, and end results program at the National Cancer Institute. *J Natl Cancer Inst* 97(13):966–975.
4. Yamauchi H, et al. (2012) Inflammatory breast cancer: What we know and what we need to learn. *Oncologist* 17(7):891–899.
5. Masuda H, et al. (2014) Long-term treatment efficacy in primary inflammatory breast cancer by hormonal receptor- and HER2-defined subtypes. *Ann Oncol* 25(2):384–391.
6. Fernandez SV, et al. (2013) Inflammatory breast cancer (IBC): Clues for targeted therapies. *Breast Cancer Res Treat* 140(1):23–33.
7. Rueth NM, et al. (2014) Underuse of trimodality treatment affects survival for patients with inflammatory breast cancer: An analysis of treatment and survival trends from the National Cancer Database. *J Clin Oncol* 32(19):2018–2024.
8. Dawood S, et al. (2011) Differences in survival among women with stage III inflammatory and noninflammatory locally advanced breast cancer appear early: A large population-based study. *Cancer* 117(9):1819–1826.
9. Hajitou A, et al. (2006) A hybrid vector for ligand-directed tumor targeting and molecular imaging. *Cell* 125(2):385–398.
10. Hajitou A, et al. (2008) A preclinical model for predicting drug response in soft-tissue sarcoma with targeted AAVP molecular imaging. *Proc Natl Acad Sci USA* 105(11):4471–4476.
11. Staquicini FI, et al. (2011) Systemic combinatorial peptide selection yields a non-canonical iron-mimicry mechanism for targeting tumors in a mouse model of human glioblastoma. *J Clin Invest* 121(1):161–173.
12. Smith TL, et al. (2016) AAVP displaying octreotide for ligand-directed therapeutic transgene delivery in neuroendocrine tumors of the pancreas. *Proc Natl Acad Sci USA* 113(9):2466–2471.
13. Paoloni MC, et al. (2009) Launching a novel preclinical infrastructure: Comparative oncology trials consortium directed therapeutic targeting of TNFalpha to cancer vasculature. *PLoS One* 4(3):e4972.
14. Cook KL, Clarke PA, Clarke R (2013) Targeting GRP78 and antiestrogen resistance in breast cancer. *Future Med Chem* 5(9):1047–1057.
15. Munro S, Pelham HR (1986) An Hsp70-like protein in the ER: Identity with the 78 kd glucose-regulated protein and immunoglobulin heavy chain binding protein. *Cell* 46(2):291–300.
16. Shin BK, et al. (2003) Global profiling of the cell surface proteome of cancer cells uncovers an abundance of proteins with chaperone function. *J Biol Chem* 278(9):7607–7616.
17. Zhang Y, Liu R, Ni M, Gill P, Lee AS (2010) Cell surface relocalization of the endoplasmic reticulum chaperone and unfolded protein response regulator GRP78/BiP. *J Biol Chem* 285(20):15065–15075.
18. Mintz PJ, et al. (2003) Fingerprinting the circulating repertoire of antibodies from cancer patients. *Nat Biotechnol* 21(1):57–63.
19. Arap MA, et al. (2004) Cell surface expression of the stress response chaperone GRP78 enables tumor targeting by circulating ligands. *Cancer Cell* 6(3):275–284.
20. Zhang J, et al. (2006) Association of elevated GRP78 expression with increased lymph node metastasis and poor prognosis in patients with gastric cancer. *Clin Exp Metastasis* 23(7-8):401–410.
21. Zhuang L, et al. (2009) Expression of glucose-regulated stress protein GRP78 is related to progression of melanoma. *Histopathology* 54(4):462–470.
22. Scriven P, et al. (2009) Activation and clinical significance of the unfolded protein response in breast cancer. *Br J Cancer* 101(10):1692–1698.
23. Györffy B, et al. (2010) An online survival analysis tool to rapidly assess the effect of 22,277 genes on breast cancer prognosis using microarray data of 1,809 patients. *Breast Cancer Res Treat* 123(3):725–731.
24. Lee E, et al. (2006) GRP78 as a novel predictor of responsiveness to chemotherapy in breast cancer. *Cancer Res* 66(16):7849–7853.
25. Deroanne CF, Hajitou A, Calberg-Bacq CM, Nusgens BV, Lapière CM (1997) Angiogenesis by fibroblast growth factor 4 is mediated through an autocrine up-regulation of vascular endothelial growth factor expression. *Cancer Res* 57(24):5590–5597.
26. Forozan F, et al. (1999) Molecular cytogenetic analysis of 11 new breast cancer cell lines. *Br J Cancer* 81(8):1328–1334.
27. Klopp AH, et al. (2010) Mesenchymal stem cells promote mammosphere formation and decrease E-cadherin in normal and malignant breast cells. *PLoS One* 5(8):e12180.
28. Giordano RJ, Cardó-Vila M, Lahdenranta J, Pasqualini R, Arap W (2001) Biopanning and rapid analysis of selective interactive ligands. *Nat Med* 7(11):1249–1253.
29. Merril CR, et al. (1996) Long-circulating bacteriophage as antibacterial agents. *Proc Natl Acad Sci USA* 93(8):3188–3192.
30. Molenaar TJ, et al. (2002) Uptake and processing of modified bacteriophage M13 in mice: Implications for phage display. *Virology* 293(1):182–191.
31. Zou J, Dickerson MT, Owen NK, Landon LA, Deutscher SL (2004) Biodistribution of filamentous phage peptide libraries in mice. *Mol Biol Rep* 31(2):121–129.
32. Hajitou A, et al. (2007) Design and construction of targeted AAVP vectors for mammalian cell transduction. *Nat Protoc* 2(3):523–531.
33. Dong D, et al. (2004) Spontaneous and controllable activation of suicide gene expression driven by the stress-inducible grp78 promoter resulting in eradication of sizable human tumors. *Hum Gene Ther* 15(6):553–561.
34. Soghomonyan S, et al. (2007) Molecular PET imaging of HSV1-tk reporter gene expression using [18F]FEAU. *Nat Protoc* 2(2):416–423.
35. Tjuvajev JG, et al. (1995) Imaging the expression of transfected genes *in vivo*. *Cancer Res* 55(24):6126–6132.
36. Hamel W, Magnelli L, Chiarugi VP, Israel MA (1996) Herpes simplex virus thymidine kinase/ganciclovir-mediated apoptotic death of bystander cells. *Cancer Res* 56(12):2697–2702.
37. Hajitou A, et al. (1998) FGF-3 and FGF-4 elicit distinct oncogenic properties in mouse mammary myoepithelial cells. *Oncogene* 17(16):2059–2071.
38. Ozawa MG, et al. (2008) Beyond receptor expression levels: The relevance of target accessibility in ligand-directed pharmacodelivery systems. *Trends Cardiovasc Med* 18(4):126–132.
39. Li J, Lee AS (2006) Stress induction of GRP78/BiP and its role in cancer. *Curr Mol Med* 6(1):45–54.
40. Lee AS (2014) Glucose-regulated proteins in cancer: Molecular mechanisms and therapeutic potential. *Nat Rev Cancer* 14(4):263–276.
41. Quinones QJ, de Ridder GG, Pizzo SV (2008) GRP78: A chaperone with diverse roles beyond the endoplasmic reticulum. *Histol Histopathol* 23(11):1409–1416.
42. Martin S, et al. (2010) Targeting GRP78 to enhance melanoma cell death. *Pigment Cell Melanoma Res* 23(5):675–682.
43. Dong D, et al. (2008) Critical role of the stress chaperone GRP78/BiP in tumor proliferation, survival, and growth in transgene-induced mammary tumor development. *Cancer Res* 68(2):498–505.
44. Miao YR, et al. (2013) Inhibition of established micrometastases by targeted drug delivery via cell surface-associated GRP78. *Clin Cancer Res* 19(8):2107–2116.
45. Mandelin J, et al. (2015) Selection and identification of ligand peptides targeting a model of castrate-resistant osteogenic prostate cancer and their receptors. *Proc Natl Acad Sci USA* 112(12):3776–3781.
46. Ferrara F, et al. (2016) Targeted molecular-genetic imaging and ligand-directed therapy in aggressive variant prostate cancer. *Proc Nat Acad Sci USA*, 10.1073/pnas.1615400113.
47. US National Research Council Committee for the Update of the Guide for the Care and Use of Laboratory Animals (2011) *Guide for the Care and Use of Laboratory Animals* (Washington, DC: National Academies Press), 8th Ed.
48. Hosoya H, et al. (2016) Integrated nanotechnology platform for tumor-targeted multimodal imaging and therapeutic cargo release. *Proc Natl Acad Sci USA* 113(7):1877–1882.
49. Lelekakis M, et al. (1999) A novel orthotopic model of breast cancer metastasis to bone. *Clin Exp Metastasis* 17(2):163–170.
50. Christianson DR, Ozawa MG, Pasqualini R, Arap W (2007) Techniques to decipher molecular diversity by phage display. *Methods Mol Biol* 357:385–406.
51. Pranjol MZ, Hajitou A (2015) Bacteriophage-derived vectors for targeted cancer gene therapy. *Viruses* 7(1):268–284.
52. Hajitou A (2010) Targeted systemic gene therapy and molecular imaging of cancer contribution of the vascular-targeted AAVP vector. *Adv Genet* 69:65–82.
53. Hajitou A, et al. (2001) Down-regulation of vascular endothelial growth factor by tissue inhibitor of metalloproteinase-2: Effect on *in vivo* mammary tumor growth and angiogenesis. *Cancer Res* 61(8):3450–3457.
54. Peacock DB, Jones JV, Gough M (1973) The immune response to thetaX 174 in man. I. Primary and secondary antibody production in normal adults. *Clin Exp Immunol* 13(4):497–513.
55. Krag DN, et al. (2006) Selection of tumor-binding ligands in cancer patients with phage display libraries. *Cancer Res* 66(15):7724–7733.

Supporting Information

Dobroff et al. 10.1073/pnas.1615288113

SI Materials and Methods

Cell Lines, Reagents, and Human Specimens. The cell lines MCF10A, BT474, SK-BR-3, MCF7, and MDA-MB-231 were purchased from the American Type Culture Collection (ATCC), and the cell line SUM190 was purchased from Asterand Bioscience. The cell line MDA-IBC-3 was obtained from The Morgan Welch Inflammatory Breast Cancer Research Program at the MDACC, and the 4T1.2 and EF43.*fgf4* cell lines were previously reported (25, 48, 49). MCF10A cells were maintained in MEGM mammary epithelial cell growth medium (Lonza); BT474 cells were maintained in Hybri-Care medium (ATCC) with 1.5 g/L sodium bicarbonate; SK-BR-3 cells were maintained in McCoy's 5a (Modified) Medium (Lonza); MCF7 and MDA-MB-231 cells were maintained in DMEM/F12 (Invitrogen Life Technologies); 4T1.2 cells were maintained in RPMI-1640 (Lonza); SUM190 and MDA-IBC-3 cells were maintained in F12 medium with insulin (1 mg/mL) and hydrocortisone (1 mg/mL) (Lifeline Cell Technology); EF43.*fgf4* cells were maintained in DMEM (Invitrogen Life Technologies) with 5 ng/mL mouse EGF and 1 µg/mL bovine insulin (both from Sigma). All media were supplemented with 10% (vol/vol) FBS (Invitrogen Life Technologies), penicillin, and streptomycin. Human cell line identities were confirmed by short tandem repeat microsatellite loci analysis. Frozen stocks of all cell lines were generated at the time of authentication and were thawed no more than 3 mo before experimental use. All cells were tested and documented to be free of *Mycoplasma* species contamination. Human recombinant GRP78 was commercially obtained from Stressgen Bioreagents. De-identified archival human IBC samples were from patients of the UNMCCC (discovery set) or the MDACC (validation set). This study adheres strictly to current medical ethics recommendations and guidelines on human research, and has been reviewed and approved by the Clinical Ethics Service, Institutional Biohazard Committee, Clinical Research Committee, and Institutional Review Board at the corresponding institutions.

IHC. FFPE samples from the University of New Mexico Human Tissue Repository were stained in a Ventana Discovery XT Biomarker Platform with standardized apparatus, reagents, and protocols provided by the manufacturer (Ventana Medical Systems). Primary anti-GRP78 rabbit monoclonal antibody (Cell Signaling Technology) was used at 1:200. FFPE samples from the Pathology Core at the MDACC were stained with 10 µg/mL anti-GRP78 antibody (Santa Cruz Biotechnology) overnight at 4 °C. Following incubation in anti-goat HRP-conjugated secondary antibody (Santa Cruz Biotechnology), signal was reveled with a DAB chromogenic substrate (Dako). Staining of patient samples was evaluated with standard pathology protocols, applying a four-value intensity score (0, none; 1+, weak; 2+, moderate; 3+, strong).

Surface Detection of Membrane-Associated GRP78 by Flow Cytometry. After harvesting by Accutase (Sigma) proteolytic digestion, SUM190 cells were incubated with Ham's F12 medium supplemented with 30% (vol/vol) FBS and 10 µg/mL purified human IgG (I2511; Sigma) for 20 min at 4 °C. Cells were washed with cold PBS, and 10^6-cell aliquots were incubated with 1 µg of phycoerythrin (PE)-conjugated mouse antiGRP78 (ab12223; Abcam) or PE-conjugated isotype control for 40 min at 4 °C in 100 µL of staining buffer (0.5% BSA in PBS). After two washes, cells were resuspended in ice-cold PBS for flow cytometry analysis (AccuriC6; BD). Data were analyzed by FlowJo v. 10.0.8 (FlowJo LLC).

Phage-Binding Assays. Phage particles were amplified in host bacteria and purified as described (50). Oligonucleotide inserts were amplified by PCR and sequenced as described (50). The BRASIL methodology (28) was performed to evaluate, validate, and quantitate cell–phage binding. A polyclonal rabbit anti-GRP78 antibody (Santa Cruz Biotechnology) and/or an unrelated isotype control antibody at the same dilution were used to evaluate competitive inhibition of phage binding as indicated.

Preparation of the Loop-Grafted GRP78-Targeting Fab. The heavy-chain CDR3 (HCDR3) domain of the original Fab (anti-tetanus toxoid) cloned into pComb3XTT was replaced with an in-frame oligonucleotide coding the WIFPWIQL [GRP78-binding (19)] peptide motif by an overlapping PCR approach. The DNA fragment encoding the light chain, the constant light chain (CL), and the variable heavy chain (VH) up to the framework region 3 (FR3) was PCR-amplified with the primers SfiIVL-F (5′-GGGCC-CAGGCGGCCGAGCTC-3′) and TTFR3-R (5′-TCTCGCAC-AATAATATATGGCCGTGTC-3′). Replacement of HCDR3 with WIFPWIQL was obtained by PCR amplification with the primers TTFR3GRP78CH1-1F (5′- GACACGGCCATATAT-TATTGTGCGAGAGTGGGGGGGGTGGATCTTCCCGTG-GATCCAGCTG GGAGGATACGCTATGGACGTCTGG-GGC-3′) and 3XTT-R (reverse). (5′-AGAAGCGTAGTCCG-GAACG-TC-3′). All amplifications were completed under standard PCR conditions with Taq polymerase (Roche). The two DNA fragments were assembled by overlap extension PCR with the primers RSC-F (5′-GAGGAGGAGGAGGAGGAGGAGGCGGGGCC-CAG-GCGGCCGAGCT-3′) and 3XTT-R.

Finally, the Fab-coding DNA was digested with SfiI, ligated into the pComb3X phagemid vector, and transformed into *Escherichia coli* strain Top10F (Invitrogen). The Fab was overexpressed in Top10F by isopropyl β-D-1-thiogalactopyranoside (IPTG) induction, purified by cobalt column (Pierce), and labeled with IRDye 800CW following the manufacturer's instructions (LI-COR).

Design, Genetic Engineering, and Production of GRP78-Targeting AAVP Particles. Experimental protocols for the generation of ligand AAVP-based vectors have been described extensively (9; reviewed in refs. 32, 51, 52). Briefly, the *CMV* promoter cassette and inverted terminal repeats were obtained from pAAV-MCS (Stratagene) and cloned into the AAVP vector by using standard molecular genetic protocols. The *hGRP78* promoter was PCR-amplified from pDRIVE01-GRP78(h) v04 (InvivoGen) with the primers 5′-CACAACGCGTGTGCGGTTACCAGCGGAAAT-GCC-3′ and 5′-CACACCTAGGGTGCCAGCCAGTTGGGC-AGCA-3′. The resulting amplicons were digested with MluI (New England Biolabs) and AvrII (New England Biolabs) and religated into the AAVP vector backbone. All vectors were purified from culture supernatant of transformed host bacteria (MC1061 *E. coli*), resuspended in PBS (pH 7.4), and centrifuged to remove residual bacterial debris. Supernatants containing AAVP particles were titrated by bacterial infection (k91Kan *E. coli*). Serial dilutions were plated onto Luria-Bertani (LB) agar plates supplemented with tetracycline and kanamycin, and the number of AAVP transduction units (TU) was determined by bacterial colony counting.

Animal Models. Six- to eight-week-old female BALB/c (immunocompetent) and BALB/c nu/nu (nude, immunodeficient) mice (Charles River Laboratory) were kept on a 12-h light/dark cycle.

Standard rodent chow and water were available ad libitum. Orthotopic tumors were produced by inoculation of the second thoracic mammary fat pad with 1×10^6 SUM190 human IBC cells (BALB/c nu/nu immunodeficient mice) or 5×10^5 EF43.*fgf4* mouse mammary tumor cells (BALB/c immunocompetent mice) in 50 μL of a 50% (vol/vol) growth factor-deprived Matrigel (BD Biosciences) solution (1:1 vol/vol in PBS). During all imaging and surgical procedures, mice were anesthetized [250 mg/kg tribromoethanol or 2% (vol/vol) isoflurane in oxygen], and their temperature was maintained at 38 °C with a heat lamp. Tumor growth was monitored closely and recorded with a caliper, and tumor volume was calculated as $(a \times b^2)/2$ cm^3 (a, long diameter; b, short diameter) as described (25, 53). The animal experiments reported in this paper were conducted in full compliance with MDACC Institutional Animal Care and Utilization Committee (IACUC) policies and procedures, which follow a strict current guide care and use of laboratory animals (47). Before the initiation of experiments, all protocols and procedures involving animals were reviewed and approved by the corresponding IACUC of the site performing the experiment.

In Vivo Tumor Imaging with GRP78-Targeting Phage Particles or Loop-Grafted GRP78-Targeting Fab. Phage particles or Fabs were labeled with IRDye 800CW and were column purified according to the manufacturer's instructions (LI-COR). Fluorescent phage localization was evaluated on cohorts of size-matched orthotopic IBC-bearing mice injected i.v. with either GRP78-targeting or control (insertless) phage (2×10^{10} TU per mouse). NIRF images were acquired using the Pearl Impulse imaging system (LI-COR) at 24 h after administration. Fab-based imaging was performed on cohorts of size-matched orthotopic tumor-bearing mice injected i.v. with IRDye 800CW-labeled GRP78-targeting or control Fab (20 μg per mouse). NIRF images were acquired serially over time with Pearl Impulse (LI-COR) at the 24, 48, and 72 h time points after Fab administration. Fluorescence signal quantification was performed using ImageJ software with standard settings.

Preclinical Theranostic Studies in Tumor-Bearing Mice. For the in vivo molecular–genetic imaging and/or suicide therapy studies, 7 d after orthotopic implantation of SUM190 cells, BALB/c nu/nu mice received two i.v. doses (1×10^{11} TU per mouse) of GRP78-targeting AAVP particles (driven by either the *CMV* or the *hGRP78* promoter) or corresponding control AAVP particles. PET imaging (inviCRO) for the detection of *HSVtk*-expressing cells was performed by a single i.v. administration of the radiolabeled nucleoside analog substrate [^{124}I]-FIAU (35). PET scans were obtained with a microPET R4 scanner (Siemens) equipped with a computer-controlled positioning bed in a 10.8-cm transaxial and 8-cm axial field of view with no septa and operating in 3D list mode. PET/CT imaging was performed with an Inveon micro-PET/CT scanner (Siemens Preclinical Solution). PET and CT image fusion and image analysis were performed on a standard software program (ASIPro version 5.2.4.0; Siemens Preclinical Solution). For signal quantification, regions of interest were drawn on digitized images, and measured values were converted from nanocuries per cubic millimeter to percent of injected dose per gram of tissue as described (34). To analyze therapeutic potential, immunocompetent BALB/c mice orthotopically implanted with isogenic mouse EF43.*fgf4* mammary tumor cells received a single i.v. dose (1×10^{11} TU per mouse) of each AAVP 5 d after tumor implantation. Treatment with GCV i.p. at 80 mg·kg^{-1}·d^{-1} was initiated 3 d after AAVP administration and was continued daily for 1 wk, when the experiments were terminated.

Statistics. Data were analyzed by two-way ANOVA, followed by Bonferroni's test (multiple comparisons) or two-tailed Student's *t* test (paired comparisons). Data are represented as the mean ± SEM unless otherwise specified. *P* values of less than 0.05 were considered statistically significant. All statistical analyses were performed with Prism 5 software, version 5.01 (GraphPad Software).

SI Discussion

The Potential for AAVP in the Clinical Setting: Signal Specificity. Virtually all imaging techniques have limitations related to nonspecific uptake of the active agent(s) in organs such as the hepato-splenic and/or the urinary systems. This uptake might jeopardize their application, especially when evaluating potential metastases (commonly to the liver). Our technology provides an intrinsic containment of these limitations to minimize nonspecific signals, thus improving the signal-to-noise ratio. Specifically, although both GRP78-targeting and control phage particles are retained avidly by the liver (Fig. 3*A*, fluorescence imaging), no *HSVtk* reporter gene expression can be observed by PET/CT (Fig. 5*B*): Because of the lack of a specific receptor on their surface, hepatic cells do not actively internalize the AAVP particles, and therefore the transcriptional activity of the vector is prevented. A further control level of transgene expression is provided by the *hGRP78* promoter, which allows expression of the *HSVtk* transgene preferentially in tumor cells where *GRP78* is transcriptionally up-regulated (Fig. 5 *B*, *C*, and *E*). Finally, the specificity of the GRP78-targeting AAVP particles is corroborated by the reported therapeutic studies, in which no distress was observed in mice caused by liver (or other organ) failure. This finding further demonstrates that the cell suicide inducing transgene *HSVtk* is not expressed at functional levels in off-target sites.

The Potential for AAVP in the Clinical Setting: Repeated Testing and Treatment. The AAVP vector is immunogenic, a characteristic that is of potential concern for applying this ligand-directed theranostic platform in the real-time monitoring of patients in response to repeated treatments. Repeated therapeutic doses of AAVP can be administered without generating neutralizing antibodies or causing distress to the patient. We previously evaluated the presence of anti-AAVP antibodies in pre- and posttreatment sera from single- and serial multidose-treated dogs. In the single-dose arm, we observed a slight increase (1.8- to 2.0-fold) in anti-AAVP antibody titers posttreatment compared with pretreatment levels. However, we did not observe any further increase over time in the serial multidose arm (day 7 vs. d 28 vs. d 56). Importantly, the presence of anti-AAVP antibodies did not affect the ability of AAVP to reduce tumor burden (13). In the present therapeutic study (Fig. 6), a single injection of AAVP was deemed sufficient because of the fast growth rate of EF43.*fgf4* tumors (~12 d to achieve a volume of 1,500 mm^3). For imaging studies (Fig. 5), two injections were performed within a 5-d interval. No adverse reaction to AAVP was observed in either scenario. In support of our present and previous data, Peacock et al. (54) and, more recently, Krag et al. (55) assessed the antibody repertoire against phage particles—the external component of our hybrid system—in both healthy adults and patients. They observed no significant immune response after serial phage infusions, and no adverse reactions were reported in individuals receiving bacteriophage injections in either study.